1 Competitive Adsorption between Propylene and Propane on Zeolite

5A and the Influence of Organic Phosphonic Acid Coatings

- 4 Xinpei Zhou, John L. Falconer, J. Will Medlin*
- 5 Department of Chemical and Biological Engineering, University of Colorado Boulder, Boulder,
- 6 CO 80309-0596, USA
- 7 * Corresponding author.
- 8 E-mail address: medlin@colorado.edu (J. Will Medlin).

9 Abstract

Understanding competitive adsorption between propylene (C ₃ H ₆) and propane (C ₃ H ₈) in
mixtures is essential for the development of an adsorptive separation process, a promising
alternative to energy-intensive distillation, to produce polymer-grade propylene. This work
investigated the selective adsorption of C ₃ H ₆ over C ₃ H ₈ on zeolite 5A using a pulse injection
method, followed by temperature-programmed desorption (TPD) to investigate desorption kinetics
In mixture adsorption on uncoated 5A, C ₃ H ₆ /C ₃ H ₈ selectivity increased markedly with cumulative
gas exposure, such that it reached ~26 from an equimolar mixture at high exposures; in contrast,
the ideal selectivity measured from single-gas adsorption was only ~1.6. TPD experiments
indicated that mixture selectivity was higher than ideal selectivity because C ₃ H ₆ , having a stronger
affinity for the zeolite, hindered C ₃ H ₈ adsorption and displaced pre-adsorbed C ₃ H ₈ . To gain further
insights into the roles of pore diffusion versus surface penetration in the separation mechanism,
zeolite 5A was also modified with tert-butylphosphonic acid (TBPA) or n-octadecylphosphonic
acid (ODPA). These coatings imposed an additional diffusion barrier that hindered C ₃ H ₈ transport
more substantially than C ₃ H ₆ , with highly dense ODPA having more effect than sterically bulky
TBPA. While the coatings were selective to C ₃ H ₆ transport, their effect on overall selectivity in
mixture adsorption was complex: initial selectivity was higher than on uncoated 5A, but the
selectivity on PA-coated zeolites did not improve as rapidly with exposure time. Thus, design of
optimal composite materials for selective adsorption must account for both barriers to gas diffusion
and competition for adsorption sites between adsorbates.

Keywords: Adsorptive separation, Zeolite, Competitive adsorption, Organic phosphonic acid coating

1. Introduction

32

33

34

35

36

37

38

39

40

41

42

43

44

45

46

47

48

49

50

51

52

53

54

The separation of propylene/propane (C₃H₆/C₃H₈) mixtures to produce polymer-grade propylene (desired purity $\geq 99.5\%$), mainly used for the manufacture of polypropylene, is of great importance [1,2]. The C₃H₆/C₃H₈ mixtures are mainly produced by steam cracking of naphtha and during fluid catalytic cracking of gas oils in refineries, with C₃H₆ purities of 50–60% and 80–87%, respectively [3]. Due to the low and similar boiling points of C₃H₆ and C₃H₈ (225.6 K and 231.2 K, respectively), the distillation separation process is energy-intensive, requiring sub-ambient temperature of 183–233 K, high pressure of 16–20 bar, and towers with 150–200 stages [4,5]. A promising energy-efficient alternative is adsorptive separation based on equilibrium uptakes (equilibrium separation), molecular sieving effect (steric separation), or adsorption rates (kinetic separation) [6–8]. In equilibrium separation for olefin/paraffin, the adsorbents generally have strong affinity towards olefin compared to paraffin. The materials which can form π -complexation with olefins are usually used, such as zeolites modified with metal cations Li-13X [9], Ag-X [10], and Cs-ZK-5 [11], metal organic frameworks (MOFs) with open metal sites Co-MOF-74 [12], Fe₂(dobdc) [13], and Cu@MIL-101(Cr) [14], and covalent organic framework (COF) hexene-covalent triazine framework (CTF) [15]. Moreover, hydrogen-bonded organic framework (HOF) HOF-16 with free -COOH sites and suitable pore confinement can selectively adsorb olefins, and its regeneration is easy due to the weak binding with olefins [16]. To utilize the sieving effect for the separation of C₃H₆ and C₃H₈, adsorbents with precisely controlled pore structures have been used, such as zeolites 4A and SAPO-14 [17], MOF materials KAUST-7 [18] and Y-abtc [3]. The MOF material JNU-3a realized high C₃H₆/C₃H₈ selectivity by featuring dynamic molecular pockets opening to one-dimension diffusion channels [19]. It was

recently reported that the local sieving channels of ZU-609 enabled high selectivity and gas diffusion rates [20]. Moreover, HOF material HOF-FJU-1 achieved high selectivity and gas capacity benefited from highly discriminating gating effect under elevated temperatures [21].

In kinetic separation, porous materials with suitable aperture windows or pore channels have been utilized, such as zeolites DD3R [22], SiCHA [23], ITQ-55 [24], and ZSM-58 [25], carbon materials CMS [26] and CNP [27], and MOF materials ELM-12 [6], ZIF-8 [28], and Zn-ATA [29]. The kinetic separation process is generally more energy-efficient than equilibrium separation for recovering C₃H₆ from adsorbents due to the absence of strong interactions, and it has less serious problems of gas diffusion and adsorbent regeneration in steric separation with strong restriction of the pore structures [6]. The adsorption selectivity of kinetic separation can be improved by tuning the pore structures of adsorbents, e.g. by functionalizing the external surfaces of adsorbents with additional diffusion layers or functional groups [30,31] or by tuning the pore openings with deposition of coatings on adsorbent surfaces [32].

Modification with self-assembled monolayers of organic phosphonic acids (PAs) is a promising method to tune the properties of metal oxide surfaces, in which covalent bonds are formed between PA and hydroxyl surface through condensation reactions [33,34]. Our previous work showed that the PA coatings on zeolite surfaces can control the relative adsorption rates of pure-component C₃H₆ and C₃H₈ by varying the molecular structure of the PAs, such as changing the alkyl chain length and steric configuration of the PAs [35,36]. Single-gas, pressure-decay adsorption measurements revealed that PA monolayers on zeolite 5A significantly enhanced the kinetic selectivity of C₃H₆/C₃H₈, and the kinetic modeling with an internal diffusion model and a surface limitation model showed that PA coatings changed the diffusion rate-limiting step from zeolite pore channels to the PA coating layers at the external surfaces of the zeolites [36]. However,

this previous study focused on the effect of PA coatings on single-gas diffusion and ideal selectivity. Further measurements, such as breakthrough and mixture adsorption selectivity, are needed to examine the performance of PA-coated zeolites as potential adsorbents for the adsorptive separation of C₃H₆/C₃H₈ in mixtures.

78

79

80

81

82

83

84

85

86

87

88

89

90

91

92

93

94

95

96

97

98

99

100

In an adsorptive separation process, the difference in interactions of gas components with adsorbent surfaces can affect mixture adsorption selectivity, which may be quite different from ideal selectivity measured with single-gas adsorption. Campo et al. [37] reported that the displacement of pre-adsorbed C₃H₈ by C₃H₆ on zeolite 13X was observed in the breakthrough curve for a 75/25 (molar ratio) C₃H₆/C₃H₈ mixture, and the authors attributed this displacement to stronger adsorption of C₃H₆ than C₃H₈ on zeolite 13X. Chai et al. [38] found that in the adsorption of an equimolar mixture of acetylene (C₂H₂) and ethylene (C₂H₄) on zeolite Ni@FAU, little C₂H₄ adsorbed, and the dynamic separation selectivity of C₂H₂/C₂H₄ was up to 100, whereas the ideal selectivity was only 1.5. Their successive adsorption experiments showed that C₂H₂ displaced preadsorbed C₂H₄ on Ni@FAU, and they ascribed this to strong binding of C₂H₂ with the zeolite; this was confirmed by differential scanning calorimetry and in situ Fourier transform infrared spectroscopy. Abedini et al. [39] reported that the mole fraction of C₃H₈ in the effluent from a 30/30/40 (molar ratio) C₃H₆/C₃H₈/Ar feed mixture was as high as 0.59 in a breakthrough measurement on Cu-MOF-74, which was higher than expected if no C₃H₆ was in the effluent. The excess C₃H₈ in the effluent was ascribed to the displacement of pre-adsorbed C₃H₈ by C₃H₆ due to the stronger affinity of adsorbent towards C₃H₆; this was confirmed by the higher heat of adsorption for C₃H₆ than C₃H₈. Similar displacement phenomenon in mixture adsorption was observed in systems using zeolite ITQ-55 [24], MOF material ZU-36-Ni [40], and HOF material HOF-FJU-1 [21].

In this work, the adsorptive separation performance of uncoated zeolite 5A and the same material coated with PAs was measured for C₃H₆/C₃H₈ mixtures and compared with single-gas adsorption measurements. We found that mixture adsorption yielded surprising improvements in selectivity, which were not apparent from prior single-gas measurements. To understand the origins of the improved selectivity, we investigated the interactions of gas components with the zeolite as a function of gas exposure by means of successive adsorption of pure-component C₃H₆ and C₃H₈ and by mixture adsorption on uncoated and PA-coated zeolite 5A. Adsorption experiments were followed by temperature-programmed desorption (TPD) to quantify gas desorption kinetics. To control the surface barriers to gas diffusion, we studied a sterically bulkier PA (*tert*-butylphosphonic acid, TBPA) and a long, linear chain PA (*n*-octadecylphosphonic acid, ODPA) on the zeolite surfaces. We found that C₃H₆/C₃H₈ selectivity was related to cumulative gas exposure and diffusion resistance through the PA coating layers on the zeolite surfaces, which may provide support for the design of adsorbents and adsorptive separation processes.

2. Experimental Methods

2.1 Materials and characterization

The PA-coated zeolite 5A used in this work was synthesized based on the procedures reported previously [35,36]. For the synthesis, 830 mg of zeolite 5A calcined at 673 K in air for 4 h was added to 200-mL solution (0.01 mol/L) of PA in tetrahydrofuran (THF), then stirred for 16 h, and centrifuged at 8000 rpm for 9 min. The solvent was decanted, and the solid was annealed at 393 K for 6 h, then rinsed with THF for four times, and dried in a vacuum oven at room temperature. Zeolite 5A (LTA type), $Ca_nNa_{12-2n}[(AlO_2)_{12}(SiO_2)_{12}]$ xH_2O (powder, <10 µm, Sigma-Aldrich 233676), tert-butylphosphonic acid (TBPA, \geq 97.5%, Acros Organics 321520050), n-octadecylphosphonic acid (ODPA, \geq 96.0%, Alfa Aesar 20645), and THF (high-performance

liquid chromatography grade, Fisher Chemical T425-4) were used as received. The uncoated zeolite 5A in the result section was zeolite 5A calcined at 673 K in air for 4 h, cooled, then put through deposition process in THF solvent without a PA modifier.

The crystal structures of the materials were characterized on an X-ray diffractometer (XRD), Rigaku Smartlab model, with a Cu K_a radiation source, using standard 2D detection from 7 to 40° (angle 2θ) with a step of 0.01° and a scan rate of 2° /min. The porosities were determined by nitrogen (\geq 99.999%, Airgas) adsorption isotherms at 77 K measured on a surface characterization analyzer, 3Flex model (Micromeritics Instruments). Based on the N₂ adsorption isotherms, the total surface areas were determined with the Brunauer-Emmett-Teller (BET) multi-point method [41] using relative pressure p/p^0 in the range of 10^{-7} –0.05. The external surface areas (pore size >2.5 nm) were determined with the t-plot method [42] using p/p^0 in the range of 0.20–0.40. The micropore size distributions were determined with the Horvath-Kawazoe (HK) method [43]. Besides the N₂ adsorption isotherms, the adsorption capacities of the materials were measured by pressure-decay adsorption using probe molecule CO₂ (≥99.999%, Airgas) at room temperature under manifold pressure of 40 kPa and by CO₂ isotherms at 300 K in the pressure range of 2–800 mmHg on an Autosorb-1 apparatus (Quantachrome Instruments) equipped with a custom LabVIEW-based data acquisition system. The thermal stability of PA modifiers was tested by TPD from 298 to 823 K with a heating rate of 8 K/min under 20 SCCM of helium carrier gas, and the gas composition from desorption was analyzed on a quadrupole mass spectrometer (MS, Balzers Prisma QME 200) interfaced to the flow system via a capillary line.

2.2 Adsorption and desorption measurements

124

125

126

127

128

129

130

131

132

133

134

135

136

137

138

139

140

141

142

143

144

145

146

High purity C_3H_6 gas (\geq 99.5%, Airgas) and C_3H_8 gas (\geq 99.5%, Airgas) were used for adsorption. In the apparatus as shown in Fig. S1, the gases were adsorbed with pulse injection over

a 200-mg fixed bed (10 mm in diameter and 5 mm in height) of uncoated or PA-coated zeolite 5A under helium carrier gas. An equimolar C₃H₆/C₃H₈ mixture was prepared by mixing 0.5 mL of each gas in a 1-mL syringe, and a 90/10 C₃H₆/C₃H₈ mixture was prepared by mixing 0.9 mL C₃H₆ with 0.1 mL C₃H₈. The cumulative gas exposure was controlled by changing the number of injections (1.0 mL per dose), and the time interval between injections was 3.6 min. The flow rate of the helium carrier gas was adjusted using a mass flow controller, in which the space time was 1.2 s for the gas passing through the bed when 20 SCCM of gas flow was used. Before adsorption measurements, the uncoated and PA-coated zeolite 5A were pretreated at 523 K for 2 h under 20 SCCM of helium carrier gas. Adsorption of pure-component C₃H₆ and C₃H₈, an equimolar C₃H₆/C₃H₈ mixture, and a 90/10 C₃H₆/C₃H₈ mixture was carried out at 298 K under atmospheric pressure. After gas adsorption, desorption rates and yields were measured by TPD from 298 to 523 K with a heating rate of 8 K/min under helium carrier gas with the same flow rate as in adsorption. Gas composition was analyzed using a mass spectrometer (Balzers Prisma QME 200). In the mass spectrometer fragmentation pattern for C₃H₈, the highest-intensity signal is from the mass/charge (m/z) 29 fragment, which is specific to C₃H₈ since C₃H₆ does not produce m/z 29. The highest-intensity signal for C₃H₆ is from m/z 41, but C₃H₈ also produces m/z 41 with weak intensity. The intensity ratio of m/z 41 to m/z 29 for C₃H₈ was determined with pure C₃H₈. For gas adsorption and desorption, the area under the signal curve for a mass fragment is proportional to the gas concentration at the bed outlet, and the gas amount was determined by calibration using 1.0 mL C₃H₆ and 1.0 mL C₃H₈, separately, without adsorbents in the bed. The selectivity (loading ratio of C_3H_6 to C_3H_8 at the same adsorption time divided by the ratio of components in the feed) was determined for single-gas adsorption measurement (ideal selectivity) and C₃H₆/C₃H₈ mixture

adsorption (mixture selectivity). The relative concentration C/C_0 (gas concentration of a species in

147

148

149

150

151

152

153

154

155

156

157

158

159

160

161

162

163

164

165

166

167

168

the effluent relative to that in the feed) in adsorption and the gas purity (gas concentration of a species relative to the total in the effluent) in sorption were determined.

2.3 TPD profile analysis

The desorption rates from TPD profiles were fit with a first-order model [44,45]. The desorption activation energy E_a and the rate constant pre-exponential factor v were determined by non-linear regression fitting of the desorption rates $-d\theta/dt$ versus temperature, where t is the desorption time, and θ is the fractional gas coverage on the zeolite (the ratio of gas loading at desorption time t to the maximum loading in adsorption). The coefficient of determination indicated the goodness of fit with experimental data.

3. Results and Discussion

3.1 Material structure

The deposition of TBPA and ODPA did not change the bulk crystalline structure of the zeolite, as shown by XRD (Fig. S2). For the uncoated and TBPA coated zeolite 5A, the N₂ adsorption isotherms exhibited reversible type I(a) behavior according to the IUPAC classification (Fig. S3A and B), which indicated microporous structures of the adsorbents; the micropores dominated the total surface areas (Table S1), and the micropore size distributions were narrow with median pore width 5.8 Å (Fig. S4). The diffusion barrier of N₂ into the ODPA-coated zeolite at 77 K was found to be extremely high (at relative pressure 0.05, only 0.12 mmol/g of N₂ adsorbed on the ODPA-coated 5A, whereas 7.6 mmol/g adsorbed on the uncoated 5A) (Fig. S3C), similar to molecular sieve ZU-609 [20], making the determination of surface area via the BET method problematic. This diffusion barrier is consistent with the expectation that the ODPA coating was highly crystalline, with a low degree of chain mobility, at the low temperature of the measurement. As an alternative to estimate the effect of the coatings on adsorption site availability, the adsorption

capacities of the materials were measured using CO₂. The equilibrium uptake of CO₂ on PA-coated 5A was similar to that on the uncoated zeolite, which indicated that PA coatings did not cover the adsorption sites in the zeolites (Figs. S5 and S6). Additionally, the PA coatings on zeolite 5A were thermally stable up to 570 K as confirmed by TPD (Fig. S7), similar to prior measured stabilities on TiO₂ [46].

3.2 Single-gas measurements

Single-gas adsorption was measured for C_3H_6 and C_3H_8 using pulse injections at 298 K, and after a series of injections, TPD measured gas desorption (Fig. S8). On uncoated 5A, the C_3H_6 loading was higher than C_3H_8 with 30 doses (1.0 mL for each dose), 2.44 \pm 0.08 and 1.50 \pm 0.20 mmol/g, respectively (Fig. 1A1). The TBPA coating did not detectably affect C_3H_6 adsorption, but it decreased the initial adsorption rate of C_3H_8 to 87% of the initial rate on uncoated 5A (Figs. 1B1, S9, S10, and Table S2). On ODPA-coated 5A, the initial adsorption rates of C_3H_6 and C_3H_8 were 54% and 12%, respectively, of those on uncoated 5A (Figs. 1C1, S9, S10, and Table S2). By slowing C_3H_8 diffusion more significantly, the ODPA coating increased C_3H_6/C_3H_8 ideal selectivity to \sim 4 at low gas exposures, whereas on uncoated 5A, it was only \sim 1.6 (Fig. S11). We previously proposed that the differences in diffusion rates of C_3H_6 and C_3H_8 in ODPA coating layer were entropically driven, where C_3H_6 had more available configurations, resulting in faster diffusion rate and higher selectivity than C_3H_8 [36].

For uncoated 5A, C_3H_6 breakthrough in single-gas adsorption took place after 8 injections, whereas C_3H_8 was detected at the outlet of the bed from the first injection (Fig. 1A2). The longer breakthrough time for C_3H_6 was ascribed to its stronger affinity for the zeolite. The TBPA coating did not measurably affect the C_3H_6 breakthrough time, and it did not strongly affect the C_3H_8 breakthrough, though a small increase in relative concentration C/C_0 of approximately 0.1

compared with the uncoated 5A was observed during the first ~6 injections of C₃H₈ (Fig. 1B2), consistent with a slightly smaller adsorption rate of C₃H₈ on TBPA-coated 5A. For ODPA-coated 5A, both C₃H₆ and C₃H₈ were detected in high concentrations at the outlet of the bed from the first injection (Fig. 1C2), indicating a significant barrier for adsorbate penetration. The effect of PA coatings on gas adsorption rates and ideal selectivity from pulse injection measurements was in agreement with the pressure-decay measurements for single-gas reported previously; the PA coatings added an adsorption barrier on the zeolite surfaces [36].

216

217

218

219

220

221

222

223

226

227 228

229 230

231

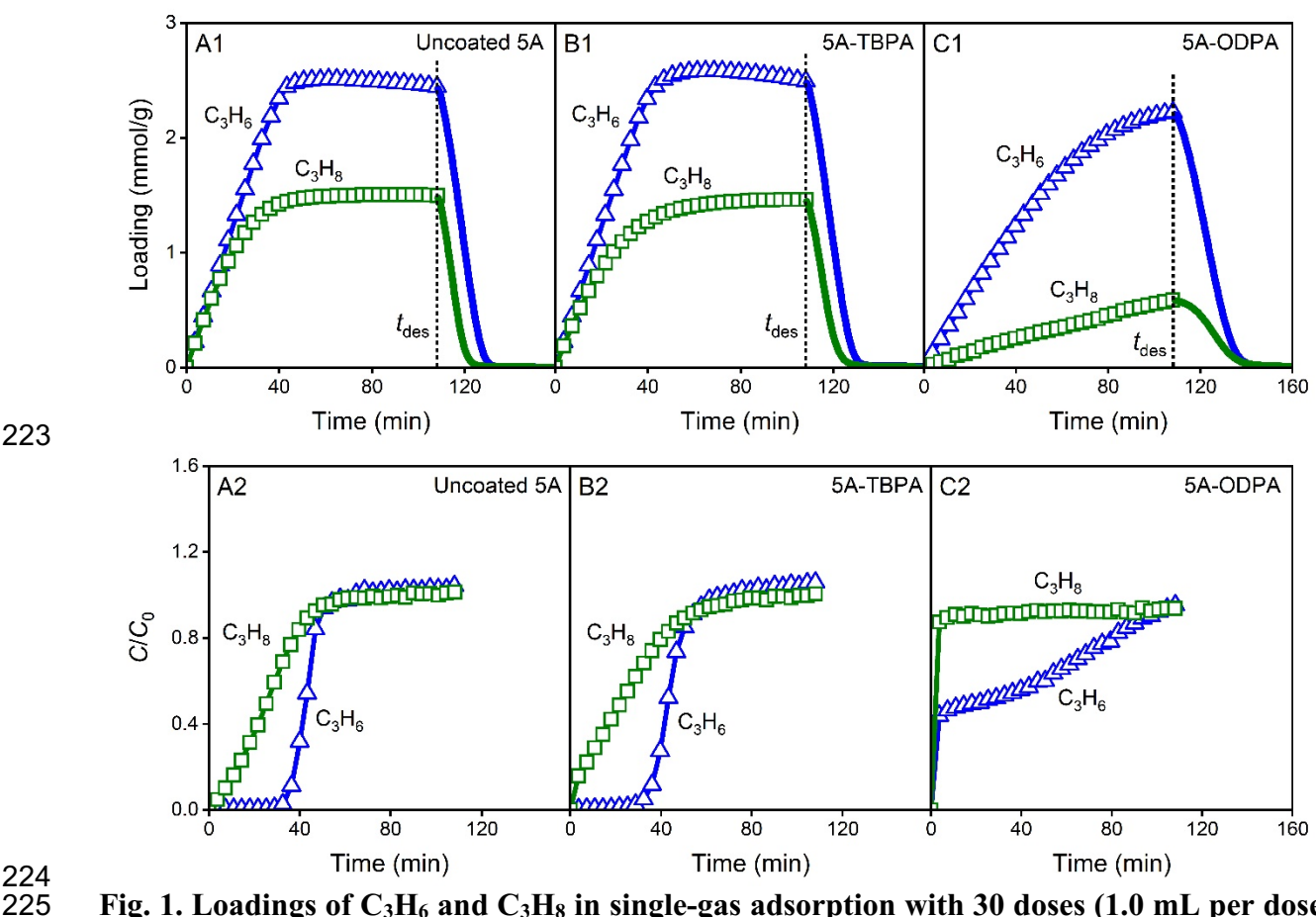


Fig. 1. Loadings of C₃H₆ and C₃H₈ in single-gas adsorption with 30 doses (1.0 mL per dose) for each gas at 298 K, followed by TPD (start at time $t_{\rm des}$), under 20 SCCM of helium, and relative concentrations C/C_0 in adsorption on (A1, A2) uncoated, (B1, B2) TBPA-, and (C1, C2) ODPA-coated zeolite 5A.

After the breakthrough measurements, desorption was carried out using TPD. The gas amount from desorption was consistent with the uptake in adsorption (Table S3). The TPD profiles (Fig.

2) showed that on uncoated 5A, the peak desorption temperature of C₃H₆ (383 K) was higher than C₃H₈ (345 K), which indicated that C₃H₆ had higher affinity for the zeolite. With a TBPA coating, the C₃H₈ desorption peak shifted to the right and broadened, with a peak temperature that increased by 6 K compared with uncoated 5A, which suggested that TBPA added a small diffusion barrier for C₃H₈ desorption, whereas it had no detectable effect on C₃H₆. On ODPA-coated 5A, the C₃H₆ peak temperature increased by 34 K compared with the uncoated zeolite, whereas the C₃H₈ peak temperature increased by 90 K, so that C₃H₈ desorbed at a higher peak temperature than C₃H₆. This indicated that diffusion in the coating layer controlled the appearance of gases from desorption, and the diffusion barrier was higher for C₃H₈ than C₃H₆.

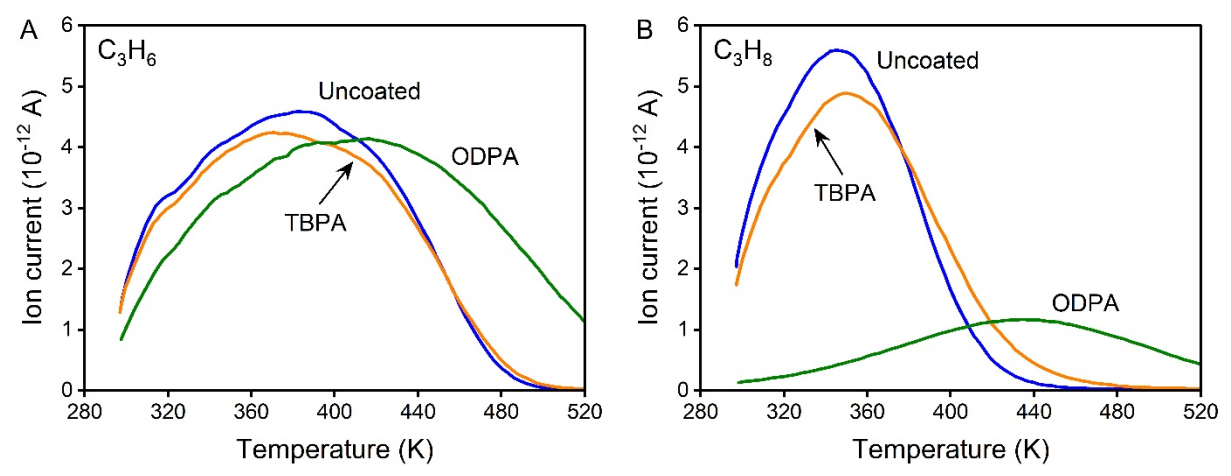


Fig. 2. TPD curves of (A) C_3H_6 and (B) C_3H_8 from uncoated, TBPA-, and ODPA-coated zeolite 5A after single-gas adsorption with 30 doses (1.0 mL per dose) for each gas at 298 K under 20 SCCM of helium.

The TPD data for uncoated and ODPA-coated zeolite 5A after single-gas adsorption with 5 doses of C_3H_6 and C_3H_8 were fit with a first-order model (Fig. 3 and Table 1) to evaluate the trends in desorption kinetics at low loadings. On uncoated 5A, the calculated apparent activation energy of C_3H_6 desorption (41.3 \pm 2.2 kJ/mol) was higher than C_3H_8 (29.9 \pm 1.1 kJ/mol). With an ODPA coating, the apparent activation energies for both C_3H_6 and C_3H_8 desorption into the vapor phase were smaller than uncoated 5A, which seems surprising since the peak temperatures were higher

on 5A-ODPA than uncoated 5A; for processes occurring through the same rate-limiting step, higher activation energies are expected to correlate with increased TPD peak temperatures. Interestingly, we found that the pre-exponential factors of the desorption rate constants for both gases were also much smaller on 5A-ODPA.

We proposed that ODPA modification changed the rate-limiting step of the desorption process from gas molecules leaving adsorption sites within the zeolite to their transport through the ODPA monolayer film [36]. The activation barrier measured for the ODPA-coated 5A corresponds to a different elementary step, diffusion through the added ODPA layer, and we proposed that the interaction enthalpies of gas molecules with PA chains were lower than with adsorption sites at zeolite internal surfaces, accounting for the small apparent activation energies of C₃H₆ and C₃H₈ desorption from 5A-ODPA. Moreover, we speculated that desorbing gas molecules experienced a large entropic penalty to diffuse through the dense ODPA coating layer, accounting for the small pre-exponential factors of desorption rate constants.

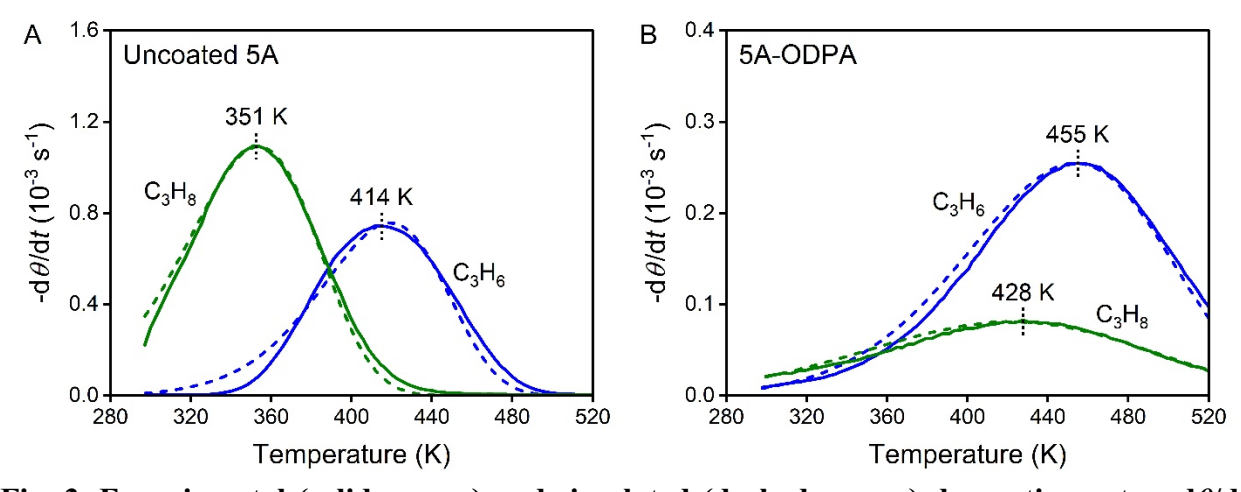


Fig. 3. Experimental (solid curves) and simulated (dashed curves) desorption rates $-d\theta/dt$ versus temperature of C_3H_6 and C_3H_8 from (A) uncoated and (B) ODPA-coated zeolite 5A after single-gas adsorption with 5 doses (1.0 mL per dose) for each gas at 298 K under 20 SCCM of helium.

Table 1 Kinetic parameters from first-order modeling of C₃H₆ and C₃H₈ TPD data after single-gas adsorption on uncoated and ODPA-coated zeolite 5A.

Adsorbent	Adsorbate	E _a (kJ/mol)	v (s ⁻¹)	Coefficient of determination
Uncoated 5A	C_3H_6	41.3 ± 2.2	$(7.0 \pm 3.3) \times 10^2$	0.99 ± 0.01
	C_3H_8	29.9 ± 1.1	$(1.3 \pm 0.6) \times 10^2$	1.00 ± 0.00
5A-ODPA	C ₃ H ₆	30.4 ± 0.6	6.3 ± 1.4	1.00 ± 0.00
	C_3H_8	17.1 ± 0.5	0.2 ± 0.1	0.99 ± 0.01

^{*} The standard deviations of kinetic parameters were determined from triplicate measurements.

3.3 Competitive adsorption on uncoated zeolite 5A

 Successive adsorption measurements were performed to investigate competitive adsorption between C₃H₆ and C₃H₈ on uncoated zeolite 5A. In the "C₃H₆-first" measurement, 10 doses of C₃H₆ were injected and 2.22 mmol/g C₃H₆ adsorbed, and then 10 doses of C₃H₈ were injected and 0.46 mmol/g C₃H₈ adsorbed. The C₃H₈ displaced 0.34 mmol/g pre-adsorbed C₃H₆; that is, 15% of the C₃H₆ was displaced (Fig. 4A and Fig. S12A). In contrast, when the dosing order was switched ("C₃H₈-first" measurement), C₃H₆ displaced 87% of pre-adsorbed C₃H₈ (Fig. 4B and Fig. S12B). Significant displacement of pre-adsorbed C₃H₈ by C₃H₆ confirmed that C₃H₆ adsorbed more strongly on uncoated 5A.

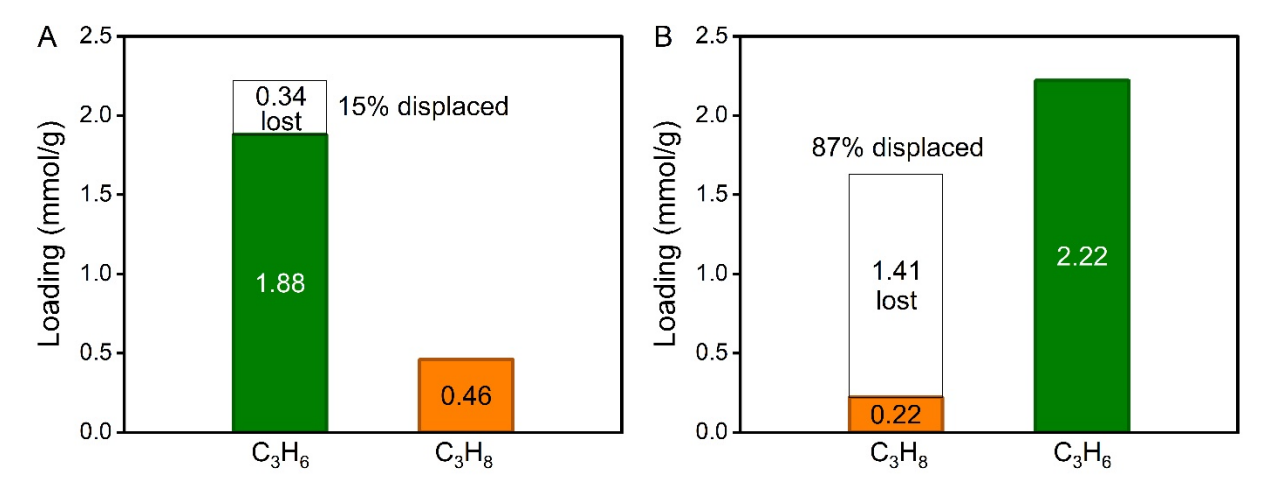


Fig. 4. Gas loadings in successive adsorption on uncoated zeolite 5A with (A) 10 doses of C_3H_6 then 10 doses of C_3H_8 (" C_3H_6 -first") and (B) 10 doses of C_3H_8 then 10 doses of C_3H_6 (" C_3H_8 -first") at 298 K under 10 SCCM of helium. In " C_3H_6 -first", C_3H_8 displaced 15% preadsorbed C_3H_6 , and in " C_3H_8 -first", C_3H_6 displaced 87% pre-adsorbed C_3H_8 .

Mixture adsorption measurements of equimolar and 90/10 (molar ratio) C₃H₆/C₃H₈ were conducted to examine the performance of zeolite 5A under competitive adsorption conditions. For equimolar mixture adsorption on uncoated 5A, as the number of mixture injections increased, the loadings of both C₃H₆ and C₃H₈ increased significantly at low numbers of injections; after 10 injections, the loading of C₃H₆ kept increasing, whereas that of C₃H₈ decreased, which indicated that C₃H₆ displaced pre-adsorbed C₃H₈ (Fig. 5A1). The concentration of C₃H₈ in the effluent relative to the feed gradually increased and was over 1.0 after 10 injections (Fig. 5A2); the excess C₃H₈ was from the displacement by C₃H₆. For a 90/10 C₃H₆/C₃H₈ mixture, C₃H₆ adsorption reached equilibrium faster than that from an equimolar mixture due to the high C₃H₆ concentration in the feed (Fig. 5B1). The adsorption selectivity from a 90/10 C₃H₆/C₃H₈ mixture was up to 23, whereas it was 12 from an equimolar mixture (Fig. S13). In the effluent, the C_3H_8 C/C_0 peak reached 1.8 in 90/10 C₃H₆/C₃H₈ mixture adsorption, indicating significant displacement of preadsorbed C₃H₈ by C₃H₆ (Fig. 5B2). Noticeably, following the adsorption of a 90/10 C₃H₆/C₃H₈ mixture, C₃H₆ gas with 99.5% purity was obtained during desorption in the collecting time represented by the interval t_i to t_f (Fig. 5C2), during which 79.1% of the desorbed C₃H₆ was collected (Fig. S14), whereas for an equimolar mixture, 46.4% of the desorbed C₃H₆ with 99.0% purity was obtained (Figs. 5C1 and S14). Overall, as indicated by Fig. S13, the exposure-dependent trends in C₃H₆ selectivity were similar across the equimolar and C₃H₆-rich feed, with a large enhancement in both cases.

290

291

292

293

294

295

296

297

298

299

300

301

302

303

304

305

306

307

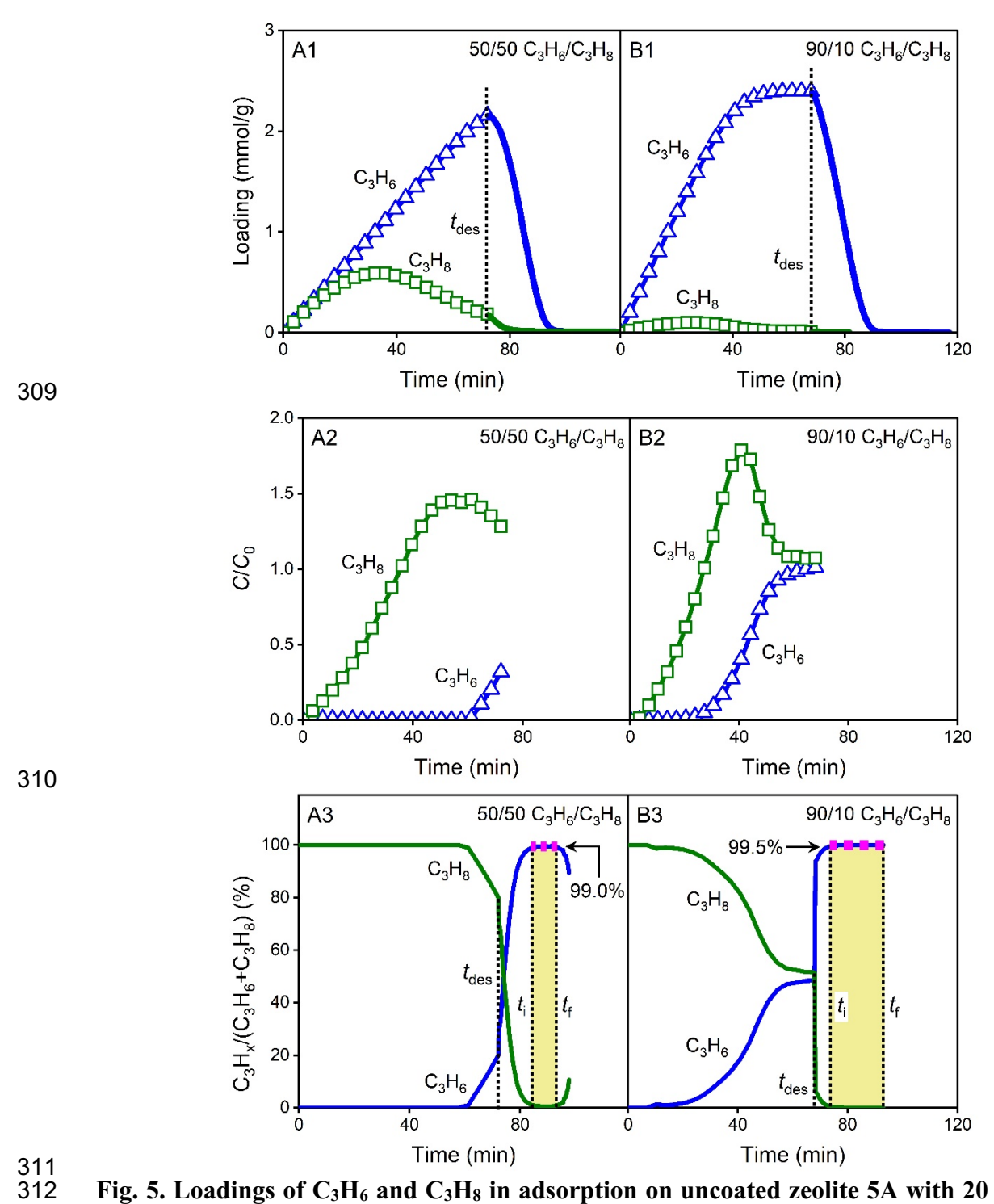


Fig. 5. Loadings of C_3H_6 and C_3H_8 in adsorption on uncoated zeolite 5A with 20 doses (1.0 mL per dose) at 298 K, followed by TPD (start at time $t_{\rm des}$), under 20 SCCM of helium, relative concentrations C/C_0 in adsorption, and gas purities in ad/desorption (dashed pink line highlighted C_3H_6 purity collected from time t_1 to t_1 in desorption) from (A1, A2, A3) an equimolar mixture and (B1, B2, B3) a 90/10 C_3H_6/C_3H_8 mixture.

The effect of flow rate of helium carrier gas on equimolar C₃H₆/C₃H₈ mixture adsorption on the uncoated zeolite 5A was investigated. With the same gas exposures, the C₃H₆ and C₃H₈ loadings under 40 SCCM of helium were lower than 10 and 20 SCCM of helium due to the lower concentrations of gases in the feed (Fig. S15A1, B1, and C1). The C₃H₆ breakthrough time was reduced with the increase of helium flow rate (Fig. S15A2, B2, and C2). Under 40 SCCM of helium, the gas concentration was low (Fig. S15C3), resulting in weak mass spectrometer signals. At a given C₃H₆ loading, a higher gas flow rate resulted in increased mixture selectivity (Fig. S16). The TPD peak of C₃H₆ shifted to low temperature and narrowed under high gas flow rate, though there was no significant difference in the C₃H₈ peak temperatures across various flow rates (Fig. S17). Considering the TPD peak shape and the intensity of mass spectrometer signals, 20 SCCM of gas flow rate was selected for the following adsorption and desorption measurements.

3.4 Influence of PA coatings on competitive adsorption

For equimolar C_3H_6/C_3H_8 mixture adsorption, similar to the uncoated 5A (Fig. 6A1 and A2), displacement behavior (with a smaller peak in C_3H_8 C/C_0) was observed for TBPA-coated 5A (Fig. 6B1 and B2), but it was not noticeable for ODPA-coated 5A within 30 doses (Fig. 6C1 and C2), perhaps because of the lower gas loadings in the ODPA-coated samples at any given number of doses. The strong competitivity of C_3H_6 adsorption was apparent even before displacement took place on any of the zeolite 5A samples: the loading of C_3H_8 in mixture adsorption was lower than that from single-gas adsorption at the same volume of C_3H_8 injected into the system, and the hindrance to C_3H_8 adsorption became more significant at higher gas exposures (Fig. S18). In desorption, the purity of C_3H_6 in the initial effluent before time point t_1 was low. After most of the C_3H_8 had desorbed, C_3H_6 gas with high purity was obtained (99.5% from uncoated zeolite 5A, 98.8% from TBPA-coated 5A, and 91.3% from ODPA-coated 5A) in collecting time represented

by the interval t_i to t_f (Fig. 6A3, B3, and C3), during which 41.3%, 41.9%, and 34.2% of the desorbed C_3H_6 were collected from those three materials, respectively (Fig. S19). The gas mixtures with C_3H_6 purity lower than polymer-grade (99.5%) need more cycles of separation [3].

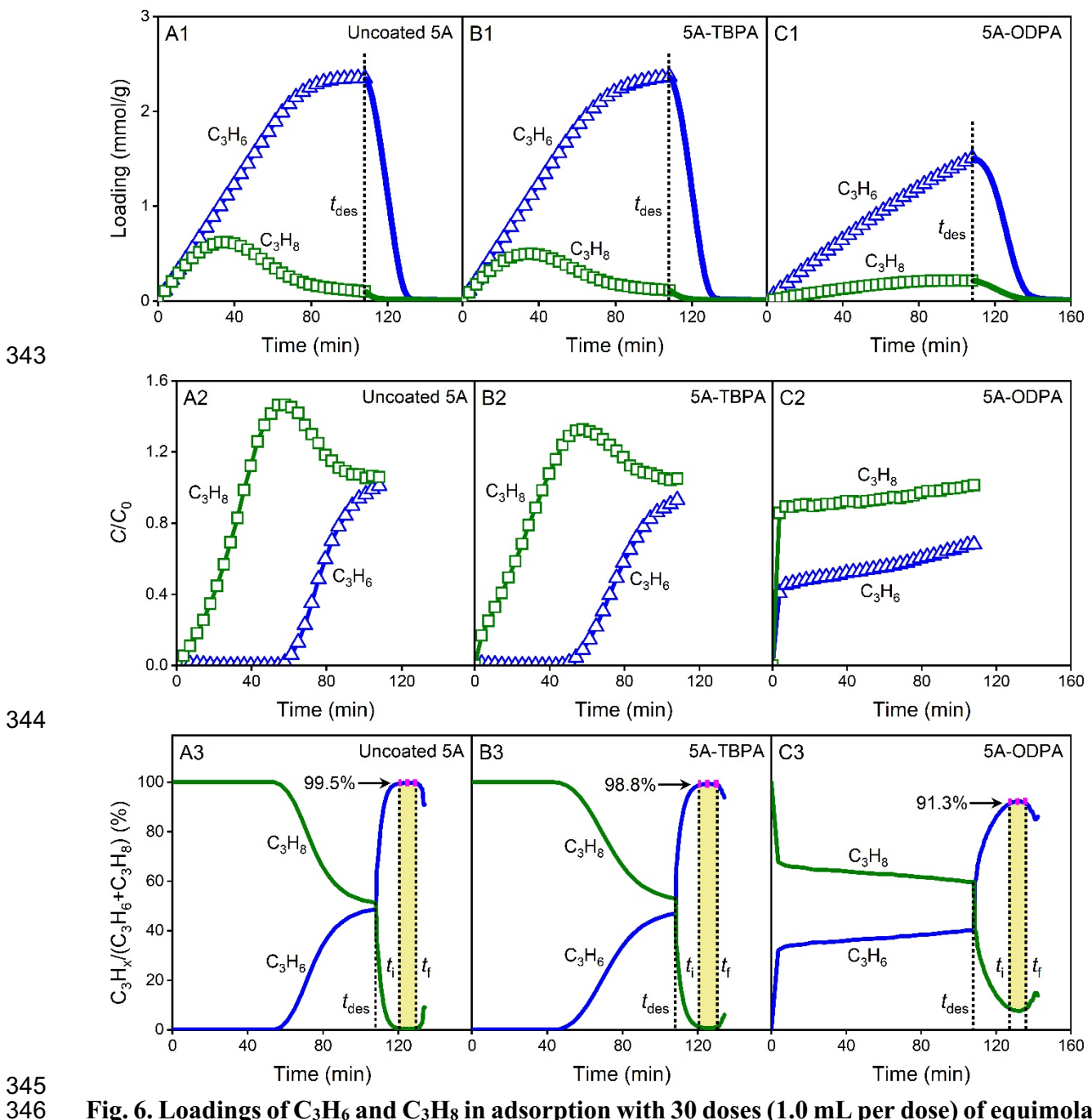


Fig. 6. Loadings of C_3H_6 and C_3H_8 in adsorption with 30 doses (1.0 mL per dose) of equimolar C_3H_6/C_3H_8 mixture at 298 K, followed by TPD (start at time $t_{\rm des}$), under 20 SCCM of helium, relative concentrations C/C_0 in adsorption, and gas purities in ad/desorption (dashed pink

line highlighted C_3H_6 purity collected from time t_i to t_f in desorption) on (A1, A2, A3) uncoated, (B1, B2, B3) TBPA-, and (C1, C2, C3) ODPA-coated zeolite 5A.

350 351 352

353

354

355

356

357

358

359

360

361

362

363

364

365

366

367

368

369

370

349

The mixture selectivities of C₃H₆/C₃H₈ from equimolar mixture adsorption on uncoated, TBPA-, and ODPA-coated zeolite 5A increased as more doses of the gas mixture were injected into the system (Fig. 7A), indicating that C₃H₆ hindered C₃H₈ adsorption and displaced preadsorbed C₃H₈. At low gas exposures, the mixture selectivity from highest to lowest was: 5A-ODPA > 5A-TBPA > uncoated 5A, whereas at high gas exposures, uncoated 5A had higher mixture selectivity than TBPA- and ODPA-coated 5A. On uncoated 5A, the mixture selectivity was up to 26 ± 2 with 30 doses of the gas mixture (Fig. 7A), whereas the ideal selectivity was only 1.6 ± 0.2 (Fig. S11). The high selectivity for the uncoated zeolite at higher gas exposures was attributed to the faster filling of the zeolite; i.e., C₃H₆ and C₃H₈ adsorbed more rapidly into the uncoated zeolite, so that a regime in which C₃H₆ displaced pre-adsorbed C₃H₈ was reached earlier in time. At a given C₃H₆ loading, 5A-ODPA had a higher mixture selectivity than the uncoated zeolite (Fig. 7B), because the ODPA coating had a larger diffusion resistance for C₃H₈ than C₃H₆. For the adsorptive separation of an equimolar mixture, the ODPA-coated zeolite 5A (C₃H₆ loading of 1.5 mmol/g, C₃H₆/C₃H₈ mixture adsorption selectivity of 8.3) and the uncoated 5A (2.3 mmol/g, 26.4) are comparable to the state-of-the-art adsorbents, such as Co-MOF-74 (6.8 mmol/g, 6.5) [12], Y-abtc (1.3 mmol/g, 8.3) [3], ZU-36-Ni (1.4 mmol/g, 19) [40], and KAUST-7 (1.3 mmol/g, 26.6) [21], at 298 K. They are also comparable to values measured for HOF-FJU-1 (2.1 mmol/g, 56.3) and JNU-3 (1.2 mmol/g, 5.9), two dynamic molecular sieving materials with a thermoregulatory gating effect, at 333 K [21]. (See Fig. 7C).

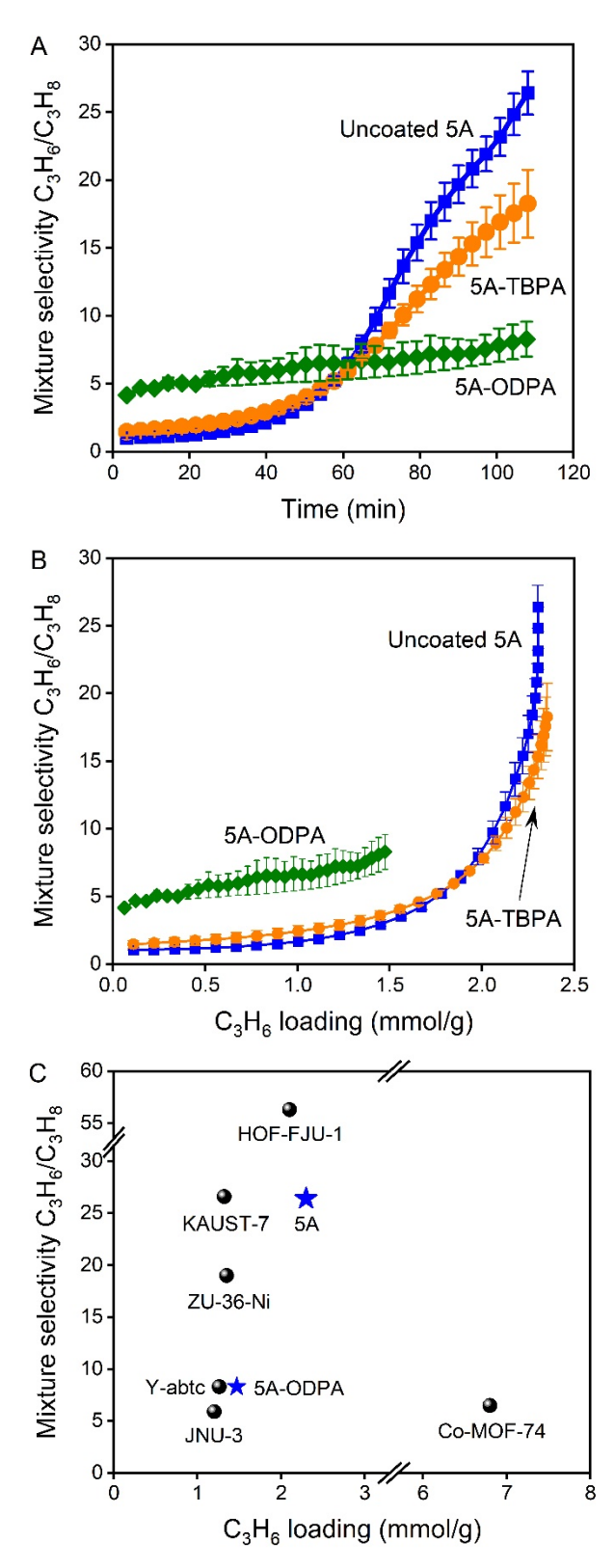


Fig. 7. Mixture adsorption selectivity versus (A) time and (B) C_3H_6 loading with 30 doses (1.0 mL for each dose) of equimolar C_3H_6/C_3H_8 at 298 K on uncoated, TBPA-, and ODPA-coated zeolite 5A. (C) Mixture selectivity against C_3H_6 loading from equimolar C_3H_6/C_3H_8

adsorption compared with state-of-the-art adsorbents (HOF-FJU-1 and JNU-3 at 333 K, and the others at 298 K).

378 379 380

381

382

383

384

385

386

387

388

389

390

391

392

393

394

395

396

397

398

399

400

401

377

3.5 TPD profiles of zeolite 5A with different coverages

To understand the difference in the affinity of C₃H₆ and C₃H₈ for zeolite 5A, the exposuredependent desorption following single-gas adsorption was considered. As shown in Fig. 8A and Table S4, on the uncoated zeolite 5A, the TPD peak temperature of C₃H₆ decreased from 414 to 380 K as the fractional coverage increased from 0.45 to 1.0, which was ascribed to the population of more weakly binding sites at higher coverages on the zeolite surfaces. In contrast, the peak temperature of C₃H₈ hardly changed with coverage, from approximately 351 to 345 K (Fig. 8B and Table S5), indicating a smaller degree of heterogeneity in the (weaker) binding sites for C₃H₈. Competitive adsorption effects in equimolar C₃H₆/C₃H₈ mixtures were also supported by TPD experiments. Similar to C₃H₆ TPD curves measured after single-gas adsorption, the C₃H₆ peak desorption temperature after mixture adsorption on the uncoated zeolite 5A decreased with increased coverage, from approximately 429 to 385 K (Fig. 8C, and Table S6). For C₃H₈, the peak temperature decreased from 351 to 309 K as the gas exposure increased in mixture adsorption (Fig. 8D and Table S7), whereas it had almost no change with coverage in C₃H₈ single-gas measurement (Fig. 8B and Table S5). We proposed that the reason for the peak temperature decrease of C₃H₈ desorption with increased gas exposure was that C₃H₆ with strong affinity for the zeolite repulsed C₃H₈ molecules on the zeolite surfaces, and the repulsion to C₃H₈ was more significant at higher gas exposures so that C₃H₈ molecules became easier to desorb from the zeolite surfaces. In other words, it appeared that even relatively weakly-binding sites in the zeolite had a significant preference for adsorption of C₃H₆. The C₃H₈ coverage calculated from TPD curves decreased as the gas exposure increased (Table S7), which was consistent with the competitive adsorption that C₃H₆ displaced pre-adsorbed C₃H₈ at high gas exposures (Fig. 6A1).

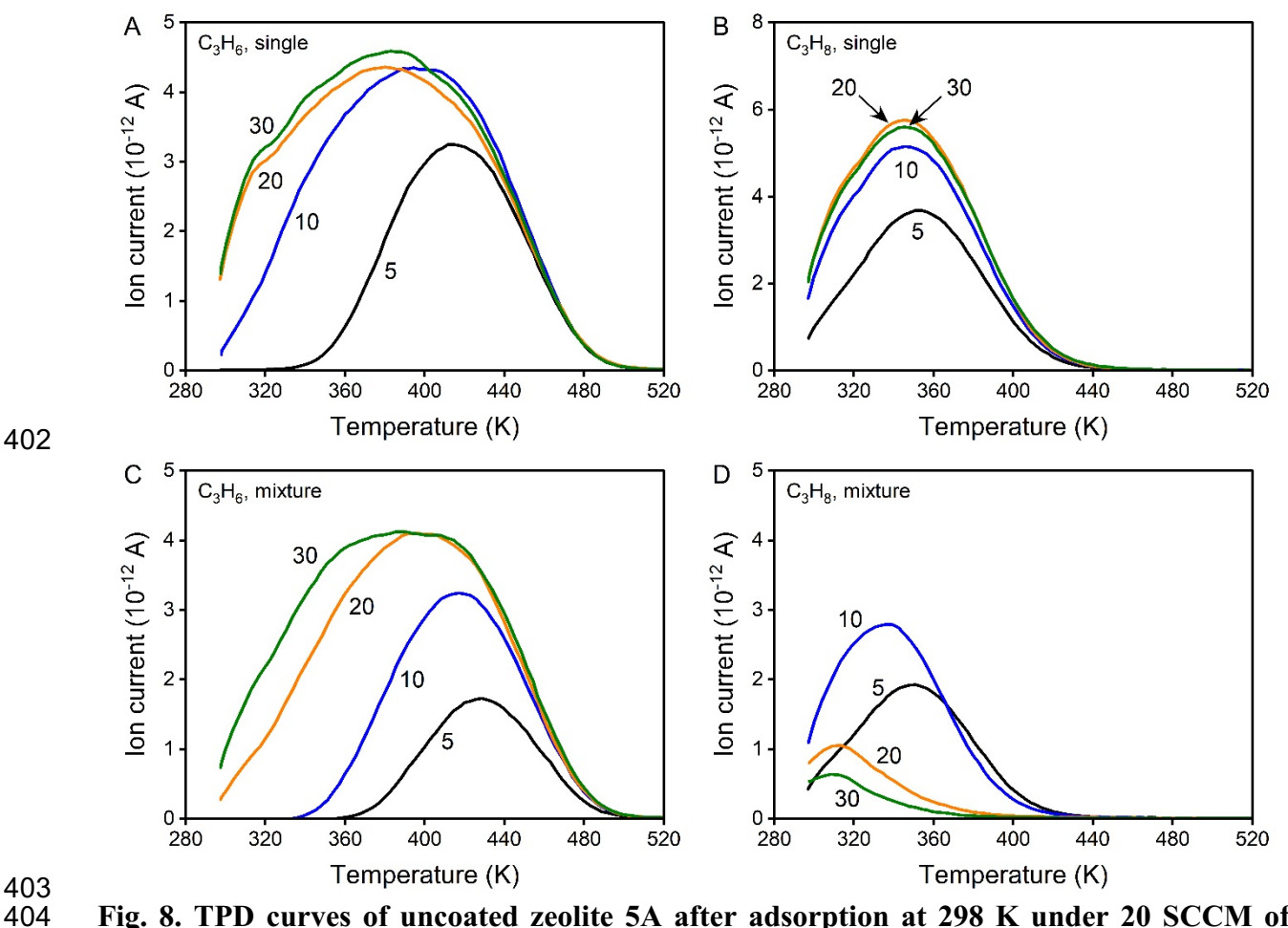


Fig. 8. TPD curves of uncoated zeolite 5A after adsorption at 298 K under 20 SCCM of helium with 5, 10, 20, 30 doses (1.0 mL per dose) of single gases: (A) C_3H_6 , (B) C_3H_8 , and equimolar C_3H_6/C_3H_8 mixture: (C) C_3H_6 , (D) C_3H_8 .

For the same TPD experiments after adsorption on ODPA-coated 5A, the peak desorption temperatures of C₃H₆ and C₃H₈ from both single-gas and mixture adsorption were higher than those on uncoated 5A (Fig. 9); the ODPA coating layers on the zeolite surfaces added resistance for diffusion of gas molecules from desorption and therefore lowered the initial desorption rate. On ODPA-coated 5A after mixture adsorption, the TPD peak temperature of C₃H₆ decreased as coverage increased (Fig. 9C and Table S10), similar to the trend for C₃H₆ single-gas measurements (Fig. 9A and Table S8). For C₃H₈ after mixture adsorption, the peak desorption temperature decreased from 438 to 394 K (Fig. 9D and Table S11), such that there was some effective "repulsion" from C₃H₆ molecules on the zeolite surfaces, especially at high coverage. In contrast,

the C₃H₈ peak temperature from single-gas measurements showed no apparent change with coverage (Fig. 9B and Table S9). Different from uncoated 5A, the displacement phenomenon on 5A-ODPA was not observed until 30 doses of mixture, and C₃H₈ loading kept increasing as the gas exposure increased (Table S11).

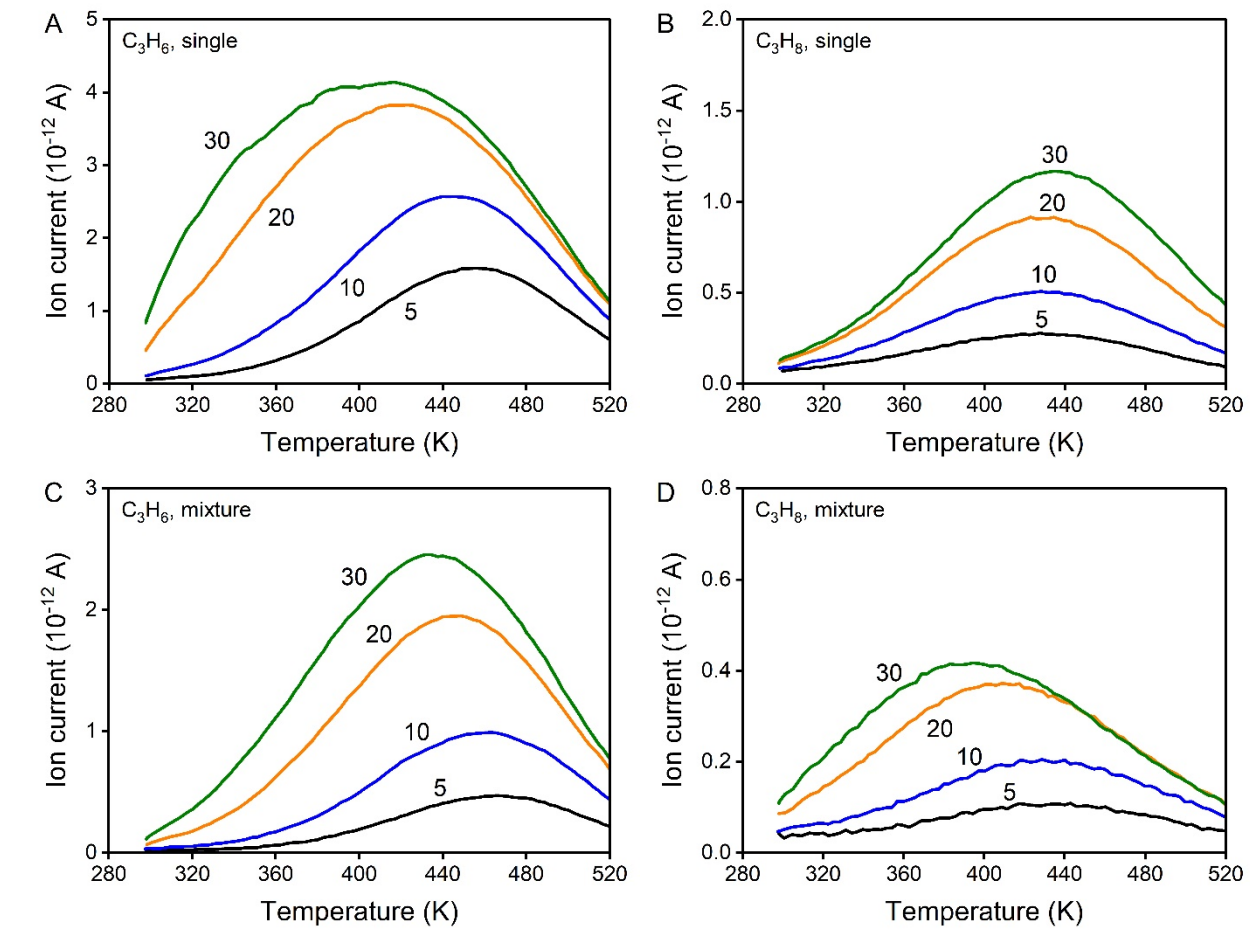


Fig. 9. TPD curves of ODPA-coated zeolite 5A after adsorption at 298 K under 20 SCCM of helium with 5, 10, 20, 30 doses (1.0 mL per dose) of single gases: (A) C_3H_6 , (B) C_3H_8 , and equimolar C_3H_6/C_3H_8 mixture: (C) C_3H_6 , (D) C_3H_8 .

In mixture adsorption, the ODPA coating enhanced the kinetic selectivity of C₃H₆/C₃H₈ by adding an additional diffusion barrier on the zeolite surfaces, but the ODPA coating lowered adsorption rates. The uncoated 5A had low initial mixture selectivity, but it had much higher mixture selectivity at high gas exposures because C₃H₆ displaced pre-adsorbed C₃H₈. The ODPA coating favored adsorption selectivity of C₃H₆/C₃H₈ at low gas exposures, whereas uncoated

zeolite 5A is a potential adsorbent for the separation at high gas exposures. Essentially, uncoated zeolite 5A allowed for high gas loadings to be achieved at earlier times, providing a thermodynamic driver for high selectivity based on the favorable adsorption of C₃H₆. Moreover, the properties of the coating played a major role in dictating the overall separation performance: whereas ODPA dramatically improved initial selectivity and suppressed adsorption rates, TBPA had much more muted effects on both parameters. Therefore, in gas separation process, there is a tradeoff between adsorption rate and selectivity for the selection of adsorbent. In addition, the operating parameters need to be optimized to improve the adsorption kinetics for industrial application, and competitive adsorption needs to be considered for the determination of operating conditions.

4. Conclusions

The performance of zeolite 5A for C_3H_6/C_3H_8 separation and the influence of PA coatings were evaluated by both single-gas and mixture adsorption using pulse injections, following by temperature-programmed desorption. In gas adsorption, C_3H_6 preferentially adsorbed on uncoated and PA-coated 5A because of the higher diffusion rate of C_3H_6 and its stronger affinity for the zeolite. The PA coatings added additional diffusion barriers on the zeolite surfaces and resulted in high mixture selectivity of C_3H_6/C_3H_8 at low gas exposures. The sterically bulkier TBPA created lower density coating layers on the zeolite surface, and it had less effect on adsorption than ODPA with a long, linear chain. While the selectivity effects of coatings on single-gas adsorption were relatively straightforward, mixed gas adsorption revealed more complex behavior. On uncoated 5A, C_3H_6 displaced pre-adsorbed C_3H_8 and resulted in high mixture selectivity, up to ~26 from an equimolar C_3H_6/C_3H_8 mixture at high gas exposures, whereas the ideal selectivity was only ~1.6. A C_3H_6 -rich mixture promoted the displacement and resulted in higher selectivity than an

equimolar mixture at the same gas exposure. For both uncoated and ODPA-coated 5A, the C₃H₈ peak desorption temperature decreased significantly after mixture adsorption compared with that after C₃H₈ single-gas adsorption, indicating that C₃H₈ desorption was promoted by the repulsion from C₃H₆ on the zeolite surfaces. Moreover, experiments in which the adsorption sequence of pure-component C₃H₆ and C₃H₈ was switched further confirmed the preferential adsorption of C₃H₆ over C₃H₈, with C₃H₆ displacing far more C₃H₈ than vice versa. The findings demonstrate the importance of competitive adsorption in dictating mixture selectivity. Comparison of the mixture adsorption performance of the ODPA-coated and uncoated zeolites revealed that use of materials having faster adsorption is not only attractive from the perspective of more rapid uptake but also, unexpectedly, can improve selectivity by enabling a faster rate of displacement of one adsorbate (propane) by another (propylene).

Author Contributions

- 468 X.Z.: data curation; writing original draft, writing-review and editing, analysis. J.L.F.:
- 469 conceptualization; methodology; funding acquisition; writing-review and editing, analysis.
- 470 J.W.M.: conceptualization; methodology; funding acquisition; supervision; writing-review and
- 471 editing, analysis.

Declaration of Competing Interest

The authors declare that they have no known competing financial interests or personal relationships that could have appeared to influence the work reported in this paper.

Acknowledgments

This work was supported by the National Science Foundation [grant CBET 1916738]. The XRD was supported by the Characterization (CHR) facility within the Colorado Shared Instrumentation in Nanofabrication and Characterization (COSINC). The authors acknowledge

- 479 Erin Dunphy at University of Colorado Boulder for carrying out the XRD measurements and
- 480 greatly appreciate Professor Kayla Sprenger's helpful comments on the data analysis in this work.

481 References

- 482 [1] A. Akah, M. Al-Ghrami, Maximizing propylene production via FCC technology, Appl. 483 Petrochem. Res. 5 (2015) 377–392. https://doi.org/10.1007/s13203-015-0104-3.
- 484 [2] D.S. Sholl, R.P. Lively, Seven chemical separations to change the world, Nature. 532 (2016) 435–437. https://doi.org/10.1038/532435a.
- H. Wang, X. Dong, V. Colombo, Q. Wang, Y. Liu, W. Liu, X. Wang, X. Huang, D.M.
 Proserpio, A. Sironi, Y. Han, J. Li, Tailor-made microporous metal-organic frameworks for
 the full separation of propane from propylene through selective size exclusion, Adv. Mater.
 30 (2018) 1805088. https://doi.org/10.1002/adma.201805088.
- 490 [4] R. Faiz, K. Li, Polymeric membranes for light olefin/paraffin separation, Desalination. 287 (2012) 82–97. https://doi.org/10.1016/j.desal.2011.11.019.
- J.R. Alcántara-Avila, F.I. Gómez-Castro, J.G. Segovia-Hernández, K.I. Sotowa, T.
 Horikawa, Optimal design of cryogenic distillation columns with side heat pumps for the propylene/propane separation, Chem. Eng. Process.: Process Intensif. 82 (2014) 112–122. https://doi.org/10.1016/j.cep.2014.06.006.
- 496 [6] L. Li, R.B. Lin, X. Wang, W. Zhou, L. Jia, J. Li, B. Chen, Kinetic separation of propylene 497 over propane in a microporous metal-organic framework, Chem. Eng. J. 354 (2018) 977– 498 982. https://doi.org/10.1016/j.cej.2018.08.108.
- D.M. Ruthven, S.C. Reyes, Adsorptive separation of light olefins from paraffins,
 Microporous Mesoporous Mater. 104 (2007) 59–66.
 https://doi.org/10.1016/j.micromeso.2007.01.005.
- 502 [8] S. Abbasi, M.R. Khosravi-Nikou, A. Shariati, Selective separation of propane from the 503 propylene-propane mixture using pure silica zeolites: A molecular dynamic simulation, 504 Chem. Eng. Process.: Process Intensif. 184 (2023) 109294. 505 https://doi.org/10.1016/j.cep.2023.109294.
- [9] C.A. Grande, J. Gascon, F. Kapteijn, A.E. Rodrigues, Propane/propylene separation with
 Li-exchanged zeolite 13X, Chem. Eng. J. 160 (2010) 207–214.
 https://doi.org/10.1016/j.cej.2010.03.044.
- [10] M. Sakai, N. Fujimaki, Y. Sasaki, N. Yasuda, M. Seshimo, M. Matsukata, Preferential adsorption of propylene over propane on a Ag-exchanged X-type zeolite membrane, ACS Appl. Mater. Interfaces. 12 (2020) 24086–24092. https://doi.org/10.1021/acsami.0c01461.
- [11] J.G. Min, K.C. Kemp, K.S. Kencana, R.R. Mukti, S.B. Hong, Dealuminated Cs-ZK-5
 zeolite for propylene/propane separation, Chem. Eng. J. 413 (2021) 127422.
 https://doi.org/10.1016/j.cej.2020.127422.
- [12] Y.S. Bae, C.Y. Lee, K.C. Kim, O.K. Farha, P. Nickias, J.T. Hupp, S.T. Nguyen, R.Q. Snurr,
 High propene/propane selectivity in isostructural metal-organic frameworks with high
 densities of open metal sites, Angew. Chem. 124 (2012) 1893–1896.
 https://doi.org/10.1002/ange.201107534.
- [13] E.D. Bloch, W.L. Queen, R. Krishna, J.M. Zadrozny, C.M. Brown, J.R. Long, Hydrocarbon separations in a metal-organic framework with open iron(II) coordination sites, Science.
 335 (2012) 1606–1610. https://doi.org/10.1126/science.1217544.
- [14] H. Abedini, A. Shariati, M.R. Khosravi-Nikou, Separation of propane/propylene mixture
 using MIL-101(Cr) loaded with cuprous oxide nanoparticles: Adsorption equilibria and
 kinetics study, Chem. Eng. J. 387 (2020) 124172. https://doi.org/10.1016/j.cej.2020.124172.

- 526 [15] C. Krishnaraj, H.S. Jena, K. Leus, H.M. Freeman, L.G. Benning, P. van der Voort, An 527 aliphatic hexene-covalent triazine framework for selective acetylene/methane and 528 ethylene/methane separation, J. Mater. Chem. A. 7 (2019) 13188–13196. 529 https://doi.org/10.1039/C8TA11722E.
- 530 [16] J. Gao, Y. Cai, X. Oian, P. Liu, H. Wu, W. Zhou, D. Liu, L. Li, R. Lin, B. Chen, A 531 Microporous hydrogen-bonded organic framework for the efficient capture and purification 532 of propylene, Angew. Chem. 133 (2021) 20563–20569. 533 https://doi.org/10.1002/ange.202106665.
- 534 [17] J. Padin, S.U. Rege, R.T. Yang, L.S. Cheng, Molecular sieve sorbents for kinetic separation 535 of propane/propylene, Chem. Eng. Sci. 55 (2000) 4525–4535. https://doi.org/10.1016/S0009-2509(00)00099-3. 536
- 537 [18] A. Cadiau, K. Adil, P.M. Bhatt, Y. Belmabkhout, M. Eddaoudi, A metal-organic 538 framework-based splitter for separating propylene from propane, Science. 353 (2016) 137– 539 140. https://doi.org/10.1126/science.aaf6323.
- 540 [19] H. Zeng, M. Xie, T. Wang, R.J. Wei, X.J. Xie, Y. Zhao, W. Lu, D. Li, Orthogonal-array 541 dynamic molecular sieving of propylene/propane mixtures, Nature. 595 (2021) 542–548. 542 https://doi.org/10.1038/s41586-021-03627-8.
- 543 [20] J. Cui, Z. Zhang, L. Yang, J. Hu, A. Jin, Z. Yang, Y. Zhao, B. Meng, Y. Zhou, J. Wang, Y. 544 Su, J. Wang, X. Cui, H. Xing, A molecular sieve with ultrafast adsorption kinetics for 545 propylene separation, Science. (2023) eabn8418. https://doi.org/10.1126/science.abn8418.
- 546 [21] Y. Chen, Y. Yang, Y. Wang, Q. Xiong, J. Yang, S. Xiang, L. Li, J. Li, Z. Zhang, B. Chen, 547 Ultramicroporous hydrogen-bonded organic framework material with a thermoregulatory 548 gating effect for record propylene separation, J. Am. Chem. Soc. 144 (2022) 17033–17040. 549 https://doi.org/10.1021/jacs.2c06585.
- 550 [22] J. Gascon, W. Blom, A. van Miltenburg, A. Ferreira, R. Berger, F. Kapteijn, Accelerated 551 synthesis of all-silica DD3R and its performance in the separation of propylene/propane 552 mixtures, Microporous Mesoporous Mater. 115 (2008) 585–593. 553 https://doi.org/10.1016/j.micromeso.2008.02.038.
- 554 [23] M. Khalighi, Y.F. Chen, S. Farooq, I.A. Karimi, J.W. Jiang, Propylene/propane separation 555 using SiCHA, Ind. Eng. Chem. Res. 52 (2013) 3877–3892. 556 https://doi.org/10.1021/ie3026955.
- 557 [24] P.J. Bereciartua, Á. Cantín, A. Corma, J.L. Jordá, M. Palomino, F. Rey, S. Valencia, E.W. Corcoran, P. Kortunov, P.I. Ravikovitch, A. Burton, C. Yoon, Y. Wang, C. Paur, J. 558 559 Guzman, A.R. Bishop, G.L. Casty, Control of zeolite framework flexibility and pore 560 topology for separation of ethane and ethylene, Science. 358 (2017) 1068–1071. 561 https://doi.org/10.1126/science.aao0092.
- 562 [25] C. Selzer, A. Werner, S. Kaskel, Selective adsorption of propene over propane on 563 hierarchical zeolite ZSM-58, Ind. Eng. Chem. Res. 57 (2018) 6609–6617. 564 https://doi.org/10.1021/acs.iecr.8b00377.
- 565 [26] J. Liu, Y. Liu, D.K. Talay, E. Calverley, M. Brayden, M. Martinez, A new carbon molecular 566 sieve for propylene/propane separations, Carbon. 85 (2015) 201–211. 567 https://doi.org/10.1016/j.carbon.2014.12.089.
- [27] S. Xu, W.C. Li, C. Wang, R. Liu, G.P. Hao, A.H. Lu, Beyond the selectivity-capacity trade-568 569 off: Ultrathin carbon nanoplates with easily accessible ultramicropores for high-efficiency 570 propylene/propane separation, Nano Lett. 22 (2022) 6615–6621.
- 571 https://doi.org/10.1021/acs.nanolett.2c01930.

- 572 [28] B.R. Pimentel, R.P. Lively, Propylene enrichment via kinetic vacuum pressure swing 573 adsorption using ZIF-8 fiber sorbents, ACS Appl. Mater. Interfaces. 10 (2018) 36323– 574 36331. https://doi.org/10.1021/acsami.8b08983.
- [29] Q. Ding, Z. Zhang, P. Zhang, J. Wang, X. Cui, C.H. He, S. Deng, H. Xing, Control of
 intracrystalline diffusion in a bilayered metal-organic framework for efficient kinetic
 separation of propylene from propane, Chem. Eng. J. 434 (2022) 134784.
 https://doi.org/10.1016/j.cej.2022.134784.
- 579 [30] C.D. Chudasama, J. Sebastian, R.V. Jasra, Pore-size engineering of zeolite A for the 580 size/shape selective molecular separation, Ind. Eng. Chem. Res. 44 (2005) 1780–1786. 581 https://doi.org/10.1021/ie0493331.
- [31] X. Xu, X. Zhao, L. Sun, X. Liu, Adsorption separation of carbon dioxide, methane and
 nitrogen on monoethanol amine modified β-zeolite, J. Nat. Gas Chem. 18 (2009) 167–172.
 https://doi.org/10.1016/S1003-9953(08)60098-5.
- [32] Q. Dong, Z. Song, F. Zhou, H. Li, M. Yu, Ultrathin, fine-tuned microporous coating
 modified 5A zeolite for propane/propylene adsorptive separation, Microporous Mesoporous
 Mater. 281 (2019) 9–14. https://doi.org/10.1016/j.micromeso.2019.02.038.
 - [33] E. Hoque, J.A. DeRose, G. Kulik, P. Hoffmann, H.J. Mathieu, B. Bhushan, Alkylphosphonate modified aluminum oxide surfaces, J. Phys. Chem. B. 110 (2006) 10855–10861. https://doi.org/10.1021/jp061327a.

588 589

590

591

592

593

594

595

596

- [34] T. Hauffman, O. Blajiev, J. Snauwaert, C. van Haesendonck, A. Hubin, H. Terryn, Study of the self-assembling of *n*-octylphosphonic acid layers on aluminum oxide, Langmuir. 24 (2008) 13450–13456. https://doi.org/10.1021/la801978a.
- [35] L.D. Ellis, S.T. Parker, J. Hu, S.F. Zaccarine, M.J. Stellato, H.H. Funke, C. Sievers, S. Pylypenko, J.L. Falconer, J.W. Medlin, Tuning gas adsorption selectivity and diffusion rates in zeolites with phosphonic acid monolayers, Cell Rep. Phys. Sci. 1 (2020) 100036. https://doi.org/10.1016/j.xcrp.2020.100036.
- [36] X. Zhou, J.L. Falconer, J.W. Medlin, Mechanism of selectivity control for zeolites modified
 with organic monolayers, Microporous Mesoporous Mater. 337 (2022) 111913.
 https://doi.org/10.1016/j.micromeso.2022.111913.
- [37] M.C. Campo, A.M. Ribeiro, A. Ferreira, J.C. Santos, C. Lutz, J.M. Loureiro, A.E.
 Rodrigues, New 13X zeolite for propylene/propane separation by vacuum swing adsorption,
 Sep. Purif. Technol. 103 (2013) 60–70. https://doi.org/10.1016/j.seppur.2012.10.009.
- [38] Y. Chai, X. Han, W. Li, S. Liu, S. Yao, C. Wang, W. Shi, I. da-Silva, P. Manuel, Y. Cheng,
 L.D. Daemen, A.J. Ramirez-Cuesta, C.C. Tang, L. Jiang, S. Yang, N. Guan, L. Li, Control
 of zeolite pore interior for chemoselective alkyne/olefin separations, Science. 368 (2020)
 1002–1006. https://doi.org/10.1126/science.aay8447.
- [39] H. Abedini, M. Asgari, M. Watt Coull, A. Shariati, M.R. Khosravi-Nikou, Efficient production of polymer-grade propylene from the propane/propylene binary mixture using Cu-MOF-74 framework, Sep. Purif. Technol. 276 (2021) 119172.
 https://doi.org/10.1016/j.seppur.2021.119172.
- [40] Z. Zhang, Q. Ding, X. Cui, X.M. Jiang, H. Xing, Fine-tuning and selective-binding within an anion-functionalized ultramicroporous metal-organic framework for efficient olefin/paraffin separation, ACS Appl. Mater. Interfaces. 12 (2020) 40229–40235.
 https://doi.org/10.1021/acsami.0c07800.
- [41] S. Brunauer, P.H. Emmett, E. Teller, Adsorption of gases in multimolecular layers, J. Am.
 Chem. Soc. 60 (1938) 309–319. https://doi.org/10.1021/ja01269a023.

- [42] J.H. de Boer, B.C. Lippens, B.G. Linsen, J.C.P. Broekhoff, A. van den Heuvel, Th.J.
 Osinga, The t-curve of multimolecular N₂-adsorption, J. Colloid Interface Sci. 21 (1966)
 405–414. https://doi.org/10.1016/0095-8522(66)90006-7.
- [43] G. Horváth, K. Kawazoe, Method for the calculation of effective pore size distribution in molecular sieve carbon, J. Chem. Eng. Japan. 16 (1983) 470–475.
 https://doi.org/10.1252/jcej.16.470.
- [44] J.L. Falconer, J.A. Schwarz, Temperature-programmed desorption and reaction:
 applications to supported catalysts, Catal. Rev. 25 (1983) 141–227.
 https://doi.org/10.1080/01614948308079666.
- [45] P.A. Redhead, Thermal desorption of gases, Vaccum. 12 (1962) 203–211.
 https://doi.org/10.1016/0042-207X(62)90978-8.

632

[46] L.D. Ellis, R.M. Trottier, C.B. Musgrave, D.K. Schwartz, J.W. Medlin, Controlling the
 surface reactivity of titania via electronic tuning of self-assembled monolayers, ACS Catal.
 7 (2017) 8351–8357. https://doi.org/10.1021/acscatal.7b02789.